

Theoretical Chemistry Accounts

In silico investigation of lactone and thiolactone inhibitors in bacterial quorum sensing using molecular modeling --Manuscript Draft--

Manuscript Number:	TCAC-D-13-00101
Full Title:	In silico investigation of lactone and thiolactone inhibitors in bacterial quorum sensing using molecular modeling
Article Type:	Regular Article
Keywords:	Quorum Sensing; lactone inhibitors; Docking; Molecular dynamics; AMBER
Corresponding Author:	Marawan M Ahmed, Bsc Swinburne University of technology Melbourne, Non-US/Canada AUSTRALIA
Corresponding Author Secondary Information:	
Corresponding Author's Institution:	Swinburne University of technology
Corresponding Author's Secondary Institution:	
First Author:	Marawan M Ahmed, Bsc
First Author Secondary Information:	
Order of Authors:	Marawan M Ahmed, Bsc Stefanie Bird, Student Feng Wang, Professor Enzo A. Palombo, Professor
Order of Authors Secondary Information:	
Abstract:	<p>In the present study, the origin of the anti-quorum sensing (QS) activities of several members of a recently synthesized and in vitro tested class of lactone and thiolactone based inhibitors were computationally investigated. Docking and molecular dynamic (MD) simulations and binding free energy calculations were carried out to reveal the exact binding and inhibitory profiles of these compounds. The higher in vitro activity of the lactone series relative to their thiolactone isosteres was verified based on estimating the binding energies, the docking scores and monitoring the stability of the complexes produced in the MD simulations. The strong electrostatic contribution to the binding energies may be responsible for the higher inhibitory activity of the lactone with respect to the thiolactone series. The results of this study help to understand the anti-QS properties of lactone-based inhibitors and provide important information that may assist in the synthesis of novel QS inhibitors.</p>
Suggested Reviewers:	<p>Chang-Guo Zhan, Professor College of Pharmacy, University of Kentucky zhan@uky.edu</p> <p>Jaime Rubio-Martinez, Professor Universitat de Barcelona (UB) and the Institut de Recerca en Química Teòrica i Computacional (IQTCUB), Martí i Franqués 1, 08028, Barcelona, Spain jaime.rubio@ub.edu</p> <p>Prasad V. Bharatam, Professor National Institute of Pharmaceutical Education and Research (NIPER), Sector-67, S. A. S. Nagar, 160 062, Punjab, India pvbharatam@nipер.ac.in</p> <p>Dawei Zhang School of Physical and Mathematical Sciences, Nanyang Technological University, Singapore, 637371, Singapore</p>

zhangdw@ntu.edu.sg

Modesto Orozco
Institut de Recerca Biomedica Parc Cientific de Barcelona Barcelona, Spain
modesto@mmb.pcb.ub.es

1
2
3
4
5
6
7
8
9
10
11
12
13
14
15
16
17
18
19
20
21
22
23
24
25
26
27
28
29
30
31
32
33
34
35
36
37
38
39
40
41
42
43
44
45
46
47
48
49
50
51
52
53
54
55
56
57
58
59
60
61
62
63
64
65

***In silico* investigation of lactone and thiolactone inhibitors in bacterial quorum sensing using molecular modeling**

Marawan Ahmed^{a,b*}, Stefanie Bird^a, Feng Wang^{a,b*} and Enzo A. Palombo^b

^aeChemistry Laboratory, Faculty of Life and Social Sciences, Swinburne University, P.O. Box 218, Hawthorn, Victoria 3122, Australia.

^b Environment and Biotechnology Centre, Faculty of Life and Social Sciences, Swinburne University, P.O. Box 218, Hawthorn, Victoria 3122, Australia.

Abstract

In the present study, the origin of the anti-quorum sensing (QS) activities of several members of a recently synthesized and *in vitro* tested class of lactone and thiolactone based inhibitors were computationally investigated. Docking and molecular dynamic (MD) simulations and binding free energy calculations were carried out to reveal the exact binding and inhibitory profiles of these compounds. The higher *in vitro* activity of the lactone series relative to their thiolactone isosteres was verified based on estimating the binding energies, the docking scores and monitoring the stability of the complexes produced in the MD simulations. The strong electrostatic contribution to the binding energies may be responsible for the higher inhibitory activity of the lactone with respect to the thiolactone series. The results of this study help to understand the anti-QS properties of lactone-based inhibitors and provide important information that may assist in the synthesis of novel QS inhibitors.

Keywords: Quorum Sensing; lactone inhibitors; Docking; Molecular dynamics; AMBER.

* Correspondence authors: mmahmed@swin.edu.au (Tel: 61-3-9214 8785) and fwang@swin.edu.au (Tel. 61-3-9214-5065).

1. Introduction

Treatment of bacterial infections is a major global challenge. Bacteria continue to develop resistance to current anti-bacterial agents and the problem is becoming more wide-spread [1-4]. It is estimated that bacterial resistance can increase mortality and morbidity by a factor of two [5]. The problem is even worse in developing countries where appropriate medical services cannot always be effectively delivered [6]. An attractive pathway to resolve the problem of resistance is targeting bacterial quorum sensing [7-11].

Quorum sensing (QS) is a communication mechanism by which bacterial cells organize biological processes that are not possible with a single bacterium, such as toxin production and biofilm formation [8,12,13]. This mechanism includes binding of specific signal “hormone-like” molecules called “auto-inducers” to specific intracellular or membrane bound receptors [8,12,14]. This binding triggers a wide range of intracellular reaction cascades in Gram positive and Gram negative bacteria to carry out the required biological process [15,14]. A typical QS system is composed of three components, (i) A bacterial synthase (e.g. LuxI) that synthesizes the “auto-inducer”, (ii) The auto-inducer which is typically an acylhomoserine lactone (AHL) derivative and (iii) A transcription regulatory protein, such as LuxR or its homologues. LuxR protein binds to DNA and activates gene expression once the level of the AHL reaches a critical threshold depending on the bacterial population density [16,17].

Various mechanisms of this AHL induced QS activation have been proposed and three mechanisms are the most widely accepted. In the first mechanism, the AHL induced conformational changes on LuxR enable LuxR to bind DNA and trigger the transcription process [18,17]. In the second mechanism, the AHL induced LuxR conformational changes relieve the repressor effect exerted by LuxR on the target genes and enable gene transcription [19,20]. In the third mechanism, extracellular AHL is detected by membrane bound receptors that trigger a wide range of intracellular reactions leading to gene expression [21,8].

Bacteria cannot easily develop an acquired resistance against QS inhibitors. As a result, QS inhibition is seen as an excellent weapon to fight against bacteria [8,16]. A number of distinct methods have been described to inhibit QS. In one of such methods, the AHL synthase is inhibited by small molecule analogues of organic compounds involved in AHL biosynthesis [22-24]. Enzymatic hydrolysis of the AHL molecule by acylases, hydrolases and lactonases has been reported as an excellent defense mechanism for other organisms against bacteria [22-24]. The third and most widely investigated method is the use of small AHL analogues that competitively inhibit AHL binding to the LuxR proteins and their homologues, such as the LasR protein [24,9,7,25-28]. These classes of inhibitors are referred to as “AHL antagonists”. In the present study, two *in vitro* tested lactone and thiolactone series of AHL antagonists are computationally investigated to understand the origin of their anti-QS activities.

1 The most commonly investigated AHL antagonists are those belonging to lactone, thiolactone and
2 furanone classes of organic compounds [24,9,7,25-29]. This is due to the structural similarities between
3 these molecules and the naturally occurring AHL auto-inducers. These auto-inducers can have different
4 structures depending on the producing organism. In most cases, the auto-inducer is composed of a five-
5 membered lactone head and an acyl group spacer connecting this head to a hydrophobic chain tail. The
6 length of the tail and its chemical structure differ between AHL derivatives and can affect the potency
7 and the intrinsic activity (agonist or antagonist) of a given AHL [27,22,30,8]. This may facilitate the
8 tuning of the effect for a given inhibitor or inducer so that it can selectively inhibit or activate a
9 particular type of bacterium. Some authors suggested the ability of several molecules to inhibit QS
10 although they are not structurally related to AHL [31].
11
12
13
14
15

16 Unfortunately, computational studies on this important class of inhibitors are rare which may be due to
17 the limited availability of crystal structures of the LuxR proteins complexed with their corresponding
18 antagonists [28,32-34]. The need for detailed investigation of QS inhibition at the molecular level is
19 necessary for the understanding of QS process and the future development of effective drugs. In the
20 current study, the binding mode of a recently synthesized and tested thiolactone group of AHL
21 antagonists against LuxR proteins [8] was investigated. Docking and molecular dynamics (MD)
22 simulations were carried out against a recently resolved X-ray crystal structure of LuxR protein from
23 *Chromobacterium violaceum* (*C. violaceum*). The *C. violaceum* LuxR protein (CviR) was co-
24 crystallized with an inhibitor from a similar study but having a lactone ring instead of thiolactone, i.e.,
25 sulphur has been replaced by its isosteric oxygen atom [7]. In addition to the reported thiolactone
26 series, the corresponding lactone analogues are computationally investigated to understand the
27 differences in binding between the two groups. Also, it has been shown that the thiolactone analogue of
28 the co-crystallized inhibitor is 10-fold less effective than the lactone inhibitor, a detailed analysis is
29 carried out to understand the basis of this difference.
30
31
32
33
34
35
36
37
38

39 2. METHODS AND COMPUTATIONAL DETAILS

40
41

42 The chemical structure of the lactone and thiolactone back bone skeleton is given in Figure 1. When
43 the X atom in the penton ring is oxygen, i.e. X=O, the structures are lactones, whereas the structures
44 become thiolactones if X=S in the same figure. The R-group at the end of the chain in the back bone
45 structure is replaced by different sixteen groups as listed in the figure, which in total produced 32
46 compounds: 16 thiolactones and 16 lactones. The thiolactone series is denoted as “**TL**”, the lactone
47 series is denoted as “**L**” as marked in the same figure, in which the original co-crystallized lactone
48 inhibitor is denoted as **L3** and its thiolactone isostere is denoted as **TL3**.
49
50
51
52

53 In the protein preparation, the crystal structure of CviR (a LuxR protein) co-crystallized with
54 chlorolactone (**L3**) antagonist was taken from the PDB (PDB entry: 3QP5) [7]. Figure 2 gives a three-
55 dimensional (3D) representation of the CviR protein monomer. The complex was prepared using the
56
57
58
59
60
61
62
63
64
65

1 protein preparation wizard in Maestro 9.2 [35]. The crystallized protein structure is a tetramer, one
2 chain is kept, and others are deleted in the present study and saturated by hydrogen atoms but the water
3 molecules are deleted. Similar to a previous study [36,37], the missing residues were added and refined
4 using Prime 3.0 [38]. The N-acetyl (ACE) and N-methyl amide (NMA) groups were added to cap the
5 uncapped N and C termini respectively. H-bond network optimization was carried out assuming a
6 neutral pH of the solution. The protonation states of titratable amino acids were assigned at the same
7 pH. An all atom impref minimization step was carried out to remove unfavorable steric clashes until a
8 convergence was reached or with a maximum RMSD of 0.3 Å from the original conformation. No
9 steric clashes were reported after the final minimization step.
10
11
12
13

14 Once the protein structure is set up, a receptor grid was prepared with the receptor grid generation
15 module in Glide 5.8 [39]. The binding site was determined as a box around the ligand that was centered
16 inside the box. Four H-bonds constraints with the nearby residues (Tyr80, Trp84 Asp97, and Ser155)
17 were set in the grid preparation.
18
19
20
21

22 Ligand molecules were optimized at the RM1 [40] semiempirical level of theory as implemented in the
23 Semiempirical module in Maestro 9.2 [35]. Ligand partial atomic electrostatic potential charges (ESP)
24 charges were assigned at the HF/cc-pVTZ level of theory using Jaguar [41].
25
26

27 Next, docking and scoring of the study employed the flexible ligand docking, which was performed
28 through the Glide extra precision mode (Glide XP) [42]. In order to increase the sampling space, a
29 maximum of 50.000 initial ligand poses were kept in the initial phase of docking. A scoring window of
30 poses within 1000 kcal·mol⁻¹ from the best scoring pose were retained, from which a maximum of 800
31 poses per ligand were subjected to 200 steps of energy minimization. A potential ligand pose was
32 considered only when at least three of the four predetermined H-bond constraints were satisfied.
33 Rescoring the docked poses was done using the Prime/MM-GBSA module in Prime 3.0; residues
34 within 6Å of the ligand were considered flexible.
35
36
37
38
39
40

41 Finally, molecular dynamics (MD) simulations were conducted for the co-crystallized lactone
42 inhibitors and its thiolactone analogues with both the dimeric and the monomeric forms of the CviR
43 protein, i.e. four inhibitor-protein complexes were simulated. That is, the **L3/TL3**-CviR monomer
44 complexes and the **L3/TL3**-CviR dimer complexes. To remove any potential bias from different
45 starting configurations, the **TL3** complexes were obtained by mutating the oxygen atom of the
46 experimentally resolved **L3** complexes to a sulphur atom.
47
48
49
50

51 The structure preparation and the following MD simulations were performed using AMBER 12
52 software package [43] applying the ff03 force field [44]. Single point calculations of the
53 corresponding inhibitors were performed at the HF/6-31G* using the Gaussian 09 program [45]. The
54 inhibitor charges and other parameters were obtained using the RESP fitting [46] procedures and the
55
56
57
58

1 general AMBER force field (GAFF) [47]. The complexes were then solvated in a box of TIP3P [48]
2 water with a buffer size of 15 Å and were neutralized by counter ions.
3

4 Each system was then subjected to four consecutive minimization steps. In each step, water molecules
5 and ions were allowed to move freely for a 1000 steps of steepest descent minimization followed by
6 4000 steps of conjugate gradient minimization holding protein and inhibitor atoms constrained to their
7 original positions by a force constant of 100 kcal·mol⁻¹Å⁻², then gradually releasing the force
8 constraints to 50, 5 and zero (no constraints) kcal·mol⁻¹Å⁻², respectively. Following minimization, two
9 consecutive steps of heating and equilibration were performed. Each system was gradually heated in
10 the NVT ensemble from 0°K to 300°K for 30 ps with a time step of 1 fs, applying a force constant of
11 10 kcal·mol⁻¹Å⁻² on the protein and inhibitor coordinates. Langevin dynamics with the collision
12 frequency γ of 1 ps⁻¹ for temperature control was employed. A further 1 ns simulation in the NPT
13 ensemble was performed to equilibrate the system density by applying a time step of 2 fs, which
14 required the use of SHAKE algorithm [49] to constrain all bonds involving hydrogen atoms. The
15 temperature was controlled using Langevin dynamics with the collision frequency γ of 1 ps⁻¹ and is
16 kept at 300°K. The pressure was kept at 1 bar by applying a Berendsen barostat with a pressure
17 relaxation time of 1 ps. Each system was again relaxed in the NVT ensemble for 20 ns followed by 30
18 ns production simulation at 300°K using Berendsen temperature control [50]. In all simulation steps,
19 long-range electrostatics were computed using the particle mesh Ewald (PME) and a 12 Å real space
20 cut-off [51]. The edge effect was removed by applying periodic boundary conditions. For MD
21 simulations of the monomeric chains, weak constraining forces were applied on the DNA binding
22 domain plus the flexible coil segments of the monomeric chain. All MD simulations were carried out
23 using the PMEMD module of AMBER12. For the binding energy evaluation from the trajectory, the
24 MM/PBSA module of AMBER12 was used and using every second frame collected from the MD
25 simulations, i.e. around 3750 snapshots were used [52].
26
27
28
29
30
31
32
33
34
35
36
37
38

39 **3. RESULTS AND DISCUSSION**

40 **3.1. Docking and scoring**

41 To the best of our knowledge, the first available X-ray crystal structure for a member of the LuxR
42 family of proteins co-crystallized with a pure antagonist is the CviR protein from *Chromobacterium*
43 *violaceum* (PDB code: 3QP5) [7]. In that study, CviR was co-crystallized with various ligands of either
44 agonistic or antagonistic activities. Agonist binding to CviR results in conformational changes and
45 activation of the dimer to bind DNA and trigger DNA transcription. The ligand induced conformational
46 changes determine the intrinsic activity of a given ligand to be either an agonist or an antagonist. In
47 addition, it has been shown that subtle ligand structural differences can affect the potency and the
48 intrinsic activity of a given ligand dramatically [27,22,30,8]. Moreover, the same ligand can work as an
49 agonist or an antagonist depending on the protein homologue and the bacterial strain [27,22,30,8].
50
51
52
53
54
55
56
57

1 These unique properties urge further and extensive theoretical and experimental work to shed the light
2 on the complex mechanism that controls QS signaling.
3

4 Figure 2 presents a solid ribbon representation of a CviR protein monomer. The protein is made of two
5 distinct domains, a Ligand Binding Domain (LBD) and a DNA Binding Domain (DBD) and the two
6 domains are connected by a short flexible coil. The LBD is the bigger domain and is composed of α -
7 helices and β -sheets while the DBD is composed of a few α -helices. The exact ligand binding site is
8 shown as a solid surface inside the LBD.
9
10
11
12

13 AHLs or their analogues are characterized by a unique “sperm-like” structure composed of two parts,
14 head and tail. The lactone head is able to form an H-bond with the nearby Trp84 residue, while the acyl
15 group forms H-bonds with Asp97, Tyr80 and Ser155. The tail part is buried in a hydrophobic pocket
16 made of Val, Leu and Ile residues. Figure 3 shows two 2D ligand interaction diagrams for an agonist
17 (PDB code: 3QP1) and an antagonist (PDB code: 3QP5).
18
19
20
21

22 Table 1 reports the docking scores for the inhibitors under study using the conventional docking scores
23 and the Prime-MM/GBSA scores. Inhibitors are given in the table according to their XP Gscore. From
24 the correlation with the available experimental IC_{50} data, the Prime MMGBSA DG bind vdW score
25 achieved the best correlation with experimentally measured IC_{50} ($r_{\text{pearson}} = 0.52$). Glide Emodel
26 performed reasonably well ($r_{\text{pearson}} = 0.49$). The thiolactone derivatives showed overall lower scores
27 than their corresponding lactone analogues, which is consistent with the experimental findings. Only
28 the XP Gscore was able to identify the original lactone inhibitor (**L3**) followed by the **TL12** thiolactone
29 derivative to be the best inhibitors among the two series.
30
31
32
33
34
35

36 Figure 4 represents the 2D and 3D interaction diagrams of some selected antagonists with the CviR
37 receptor. In general, antagonists binding modes to the receptor are similar to the original co-crystallized
38 antagonist. This is a result of the strict docking criteria which are applied for accepting poses. The
39 lactone carbonyl forms a direct H-bond with the conserved Trp84 residue, the acyl group –NH forms
40 an H-bond with Asp97 and the carbonyl oxygen forms H-bonds with Tyr80 and Ser155. As the
41 libraries are focused, subtle ligand differences which are correlated directly with inhibitory activity
42 need to be paid greater attention.
43
44
45
46
47

48 The main difference between the two libraries is the isosteric replacement of the “S” atom in the **TL**
49 series by an “O” atom in the **L** series. The observed activity differences between the two libraries may
50 be related to the H-bond strength that may exist between the sulphur or oxygen ring atoms and the
51 nearby $-C_{(7)}H$ of Trp84. However, it is known that heterocyclic H-bond acceptors are grouped in the
52 “weak H-bond” category of acceptors [53]. Therefore, potential large effects of this H-bond (if any) are
53 not expected. The effect of this substitution is discussed in detail in section 3.2.
54
55
56
57
58
59
60
61
62
63
64
65

1 The major difference between any pair of inhibitors within the same library (**TL** or **L**) is the chemical
2 structure of the hydrophobic tail chain. Studies have indicated that the structure and the length of this
3 chain can affect the potency and the intrinsic activity of a given ligand [27,22,30,8]. In the two
4 inhibitor libraries, the terminal aromatic group forms a direct, sandwich type π - π stacking interaction
5 with Tyr88 aromatic ring. Assuming all inhibitors have a similar binding mode, the overall binding
6 strength (within a given library) is directly correlated with the strength of this π - π stacking interaction.
7
8
9

10 As can be seen in Table 1, substitution with Electron Donating Groups (**EDG**), such as methoxy
11 groups, resulted in a dramatic reduction in the activity regardless of the position of this substitution.
12 They also had the overall worst docking scores. For example, the IC₅₀ of –meta (**TL10**) and –para
13 (**TL7**) substituted methoxy group derivatives are 37 μ M and 11 μ M, respectively. On the other hand,
14 Electron Withdrawing Group (**EWG**) derivatives, such as halogenated derivatives, have the highest
15 inhibitory effect and best docking scores as well. For example, the top scoring inhibitors (according to
16 the Glide XP score) were the **L3** and the **TL12** inhibitors, which have IC₅₀ values of 0.38 μ M and 0.63
17 μ M, respectively. The lactone derivative of **TL12**, the **L12** antagonist, exhibited a higher XP Gscore (-
18 10.02). This makes the halogenated derivatives, particularly the poly-halogenated ones, better
19 candidates for further synthesis and biological testing.
20
21
22
23
24
25
26

27 **3.2. Molecular dynamic simulations**

28
29
30 A difficult challenge in performing a meaningful MD simulation for LuxR proteins (including CviR) is
31 their inherent flexibility. This inherent flexibility is obvious knowing that the protein can adopt
32 different conformations depending on their activation states as well as the accompanying ligand. This
33 flexibility enables different proteins to carry out their functions properly [54]. CviR is a homo-dimer
34 composed of two identical and overlapping chains of about 250 amino acids each. Each monomeric
35 chain is composed of an LBD connected to a DBD through a highly flexible coil.
36
37
38
39
40

41 An accurate measure to assess the stability of the protein complexes during MD simulations is the root
42 mean square deviations (RMSD). Figure 5 (a-b) displays the RMSD plots for the C α atoms of each
43 protein in the production simulation period. As can be seen in the plots, the **L3** complexes, in both the
44 monomeric and dimeric forms, have higher stabilities than their **TL3** counterparts. The average RMSD
45 for **L3**-CviR dimer is ~ 1.6-1.8 Å. For the **TL3**-CviR dimer complex, the average RMSD value is
46 higher with an average value of ~4 Å. This illustrates the enhanced stability of the CviR dimer with **L3**
47 over **TL3**. Interestingly, the same is true for the monomeric case such that the **L3** complex with the
48 monomeric CviR is more stable than its **TL3** counterpart.
49
50
51
52
53

54 To examine the origin of this reduced stability of the **TL3** complexes with respect to the **L3** complexes,
55 a more detailed analysis on a per-residue basis was conducted using the per-residue heavy atoms
56
57
58
59
60
61
62
63
64
65

1 RMSFs (root mean square fluctuations). Figure 6(a-b) displays the heavy atoms RMSF plots of the four
2 complexes during the simulation time. As can be seen, the **L3** complexes show enhanced stability over
3 the **TL3** complexes. For the CviR dimer complexes, the LBDs of both chains (A and B) possess an
4 overall lower RMSF during the simulation period than the DBDs. For the monomeric complexes with
5 **L3** and **TL3**, and as a result of the weak constraints applied on the “DBD+coil” segment of the
6 monomeric chains, the whole monomer is of a comparable RMSF value. The enhanced flexibility of
7 the DBD segment of the dimeric protein is expected given the fact that this segment is responsible for
8 binding to DNA upon activation [55]. It would be also interesting to investigate the detailed binding
9 event of this segment to DNA upon agonists or antagonists binding. However, such a complex process
10 is beyond the capability of conventional MD simulation and other MD paradigms, such as accelerated
11 MD, may be more suitable [56]. Research in this direction is currently in progress.
12
13
14
15
16
17

18 It is important to study the stability of the observed H-bonds as a function of the simulation time. Thus,
19 Figure 7 (a-d) displays some selected H-bonds monitored during the simulation time for the four
20 complexes. The first and most important H-bond is the one formed with Trp84 residues and it has been
21 already identified in the docking section. As can be seen in Figure 7, the average value for this H-bond
22 is ~ 1.9-2.3 Å for all complexes. The **L3** complexes have less fluctuation during the simulation time
23 than their **TL3** counterparts. The same is true for the H-bonds formed with the Tyr80 residue in all
24 complexes. For the **L3** and **TL3** complexes with the monomeric CviR chains, higher fluctuations of up
25 to 3.5 Å (**L3**) and 4.3 Å (**TL3**) were observed. Interestingly, and in most cases, the H-bond which is
26 observed via docking between the amide carbonyl and the Ser155 residue is not stable in the MD
27 simulation and the adopted rotamer shifts the –OH group to the other side (Figure 8).
28
29
30
31
32
33

34 **3.3. Total and decomposed MM-PB/GBSA binding energies**

35
36
37 Table 2 reports the binding energy scores for **L3** and **TL3** inhibitors according to the AMBER-
38 MMPB/GBSA scores as implemented in AMBER12. The AMBER-MMPB/GBSA binding energy
39 scores take the advantage of statistical averaging over many potential conformations that are produced
40 from the MD trajectories. In the AMBER-MMPB/GBSA calculations, only the inhibitor-dimer
41 complexes are considered. To further enhance statistical precision and knowing that each complex
42 contains two inhibitors, each inhibitor is treated separately as a ligand in a separate run. Final data
43 reported are the average values of the two independent AMBER-MMPB/GBSA calculations for each
44 complex.
45
46
47
48
49

50
51 As can be seen in Table 2, the major term that favors the binding for both inhibitors is the vdW
52 lipophilic term (ΔE_{vdW}). Interestingly, although the vast majority of the binding site residues are
53 lipophilic residues, the electrostatic (ΔE_{ele}) term still exhibits a significant contribution to the binding.
54 This large contribution emphasizes the importance of the H-bond interactions which are electrostatic in
55
56
57

1 nature. It would be also interesting to use certain advanced techniques, such as alanine-scanning
2 [57,58], to study the effect of mutations in residues responsible for these H-bonding interactions.
3 Research in this direction is currently in progress.
4

5
6 For **TL3**, the ΔE_{vdw} interaction is given by $-46.56 \text{ kcal}\cdot\text{mol}^{-1}$, this value is slightly higher than that for
7 **L3** which is given by $-45.31 \text{ kcal}\cdot\text{mol}^{-1}$. On the other hand, **L3** exhibits a larger contribution from the
8 ΔE_{ele} term ($-33.54 \text{ kcal}\cdot\text{mol}^{-1}$) than **TL3** (-28.37) i.e., $\Delta\Delta E_{\text{ele}}$ is equal to $5.17 \text{ kcal}\cdot\text{mol}^{-1}$ which is almost
9 equal to the energy contribution of a full H-bond. This larger contribution of the ΔE_{ele} term for **L3** than
10 **TL3** may be responsible for the fact that **L3** is ~ 10 times more active than **TL3** in the *in vitro* assay
11 [8,7]. Regarding total binding energies as expressed by the ΔG values, **L3** shows higher binding energy
12 according to the AMBER-MM/PBSA score ($-63.54 \text{ kcal}\cdot\text{mol}^{-1}$) than **TL3** ($-59.11 \text{ kcal}\cdot\text{mol}^{-1}$). The same
13 is true for the AMBER-MM/GBSA score of **L3** ($-48.65 \text{ kcal}\cdot\text{mol}^{-1}$) compared to that for **TL3** (-47.60
14 $\text{kcal}\cdot\text{mol}^{-1}$).
15
16
17
18
19
20

21 Decomposition of the binding energy on a per-residue basis is very important to understand the binding
22 mode and assess the role of each residue in the binding. Figure 9 displays the per-residue binding
23 energy analyses for the two complexes during the simulation period. For the ΔE_{vdw} and the ΔE_{ele}
24 interaction terms, only residues showing large contributions are selected. Figure 9a displays the per-
25 residue contribution for the ΔE_{vdw} interaction term. As can be seen, the major contribution to the ΔE_{vdw}
26 term is from the Tyr88 via a strong π - π stacking interactions, consistent with the observations from the
27 docking study. The contribution of this residue to the ΔE_{vdw} term for both inhibitors is similar, -2.57
28 $\text{kcal}\cdot\text{mol}^{-1}$ for **L3** and $-2.59 \text{ kcal}\cdot\text{mol}^{-1}$ for **TL3**. This is because the terminal aromatic ring which is
29 responsible for the π - π stacking interaction with this residue is identical in both inhibitors (**L3** and
30 **TL3**). The second most important ΔE_{vdw} interaction is from the Trp111 residue which contributes more
31 to **TL3** ($-2.13 \text{ kcal}\cdot\text{mol}^{-1}$) than to **L3** ($-1.96 \text{ kcal}\cdot\text{mol}^{-1}$) as a result of the presence of the more lipophilic
32 sulphur in **TL3** instead of oxygen in **L3**.
33
34
35
36
37
38
39
40

41 Figure 9b displays the per-residue contribution for the ΔE_{ele} interaction term. The most important
42 residue is Asp97 which contributes almost equally for the two inhibitors ($-11.83 \text{ kcal}\cdot\text{mol}^{-1}$ for **L3** and -
43 $11.35 \text{ kcal}\cdot\text{mol}^{-1}$ for **TL3**). Differentiation for the ΔE_{ele} term between the two inhibitors is from the
44 Tyr80 and Trp84 residues which show the highest discrepancy between the two inhibitors. For **L3**, the
45 ΔE_{ele} contributions from the Tyr80 and the Trp84 residues are $-3.37 \text{ kcal}\cdot\text{mol}^{-1}$ and $-2.88 \text{ kcal}\cdot\text{mol}^{-1}$,
46 respectively. For **TL3**, the contributions of these two residues are $-1.87 \text{ kcal}\cdot\text{mol}^{-1}$ and $-2.03 \text{ kcal}\cdot\text{mol}^{-1}$,
47 respectively. The $\Delta\Delta E_{\text{ele}}$ contribution between the two inhibitors from these two residues together is
48 $2.35 \text{ kcal}\cdot\text{mol}^{-1}$ which is almost half of the energy contribution of a full H-bond. This emphasizes the
49 importance of these two residues for any future development of CviR antagonists.
50
51
52
53
54
55
56
57
58
59
60
61
62
63
64
65

4. CONCLUSIONS

1
2 The exact binding modes of a series of recently synthesized and *in vitro* tested potential QS inhibitors
3 were investigated *in silico*. Consistent with the experimentally measured IC₅₀ values, this molecular
4 modeling study using docking scores and energies of binding showed that the lactone based inhibitors
5 indeed exhibit stronger binding properties than the thiolactone based class of inhibitors. Molecular
6 dynamics simulations of different inhibitor-protein complexes further indicated that the lactone based
7 inhibitors were more stable than the thiolactone based ones. Relative to the number of hydrophilic
8 residues present in the binding site, the electrostatic effect made a significant contribution to the
9 binding for the two series of inhibitors. Certain residues, such as Tyr80 and Trp84, were discriminating
10 between the two series of inhibitors with a larger electrostatic contribution for the lactone than the
11 thiolactone inhibitors.
12
13
14
15
16

ACKNOWLEDGEMENTS

17
18
19
20
21 MA acknowledges the Swinburne University Postgraduate Research Award (SUPRA). FW thanks the
22 National Computational Infrastructure (NCI) at the Australian National University under the Merit
23 Allocation Scheme (MAS), the Victorian Partnership for Advanced Computing (VPAC), Swinburne
24 University supercomputing (Green/gSTAR) and the Victorian Life Sciences Computation Initiative
25 (VLSCI) facilities.
26
27
28
29
30
31
32
33
34
35
36
37
38
39
40
41
42
43
44
45
46
47
48
49
50
51
52
53
54
55
56
57
58
59
60
61
62
63
64
65

References

1. Levy SB, Marshall B (2004) Antibacterial resistance worldwide: causes, challenges and responses. *Nat Med* 10:122-129.
2. Levy SB (2001) Antibiotic Resistance: Consequences of Inaction. *Clin Infect Dis* 33:124-129.
3. Levy SB (2002) Factors impacting on the problem of antibiotic resistance. *J Antimicrob Chemother* 49:25-30.
4. Aiello AE, Larson E (2003) Antibacterial cleaning and hygiene products as an emerging risk factor for antibiotic resistance in the community. *The Lancet infectious diseases* 3:501-506.
5. Holmberg SD, Solomon SL, Blake PA (1987) Health and economic-impacts of antimicrobial resistance *Reviews of Infectious Diseases* 9:1065-1078.
6. Okeke IN, Laxminarayan R, Bhutta ZA, Duse AG, Jenkins P, O'Brien TF, Pablos-Mendez A, Klugman KP (2005) Antimicrobial resistance in developing countries. Part I: recent trends and current status. *The Lancet infectious diseases* 5:481-493.
7. Chen G, Swem Lee R, Swem Danielle L, Stauff Devin L, O'Loughlin Colleen T, Jeffrey Philip D, Bassler Bonnie L, Hughson Frederick M (2011) A Strategy for Antagonizing Quorum Sensing. *Mol Cell* 42:199-209.
8. Swem LR, Swem DL, O'Loughlin CT, Gatmaitan R, Zhao B, Ulrich SM, Bassler BL (2009) A quorum-sensing antagonist targets both membrane-bound and cytoplasmic receptors and controls bacterial pathogenicity. *Mol Cell* 35:143-153.
9. Galloway WRJD, Hodgkinson JT, Bowden SD, Welch M, Spring DR (2011) Quorum sensing in Gram-negative bacteria: Small-molecule modulation of AHL and AI-2 quorum sensing pathways. *Chem Rev* 111:28.
10. Suga H, Smith KM (2003) Molecular mechanisms of bacterial quorum sensing as a new drug target. *Curr Opin Chem Biol* 7:586-591.
11. Kalia VC, Purohit HJ (2011) Quenching the quorum sensing system: potential antibacterial drug targets. *Crit Rev Microbiol* 37:121-140.
12. Waters CM, Bassler BL (2005) Quorum sensing: cell-to-cell communication in bacteria. *Annu Rev Cell Dev Biol* 21:319-346.
13. Deep A, Chaudhary U, Gupta V (2011) Quorum sensing and bacterial pathogenicity: From molecules to disease. *Journal of Laboratory Physicians* 3:4-11.
14. Reading NC, Sperandio V (2006) Quorum sensing: the many languages of bacteria. *FEMS Microbiol Lett* 254:1-11.
15. Miller MB, Bassler BL (2001) Quorum sensing in bacteria. *Annu Rev Microbiol* 55:165.
16. Bottomley MJ, Muraglia E, Bazzo R, Carfi A (2007) Molecular insights into quorum sensing in the human pathogen *Pseudomonas aeruginosa* from the structure of the virulence regulator LasR bound to its autoinducer. *J Biol Chem* 282:13592-13600.
17. Rasmussen TB, Bjarnsholt T, Skindersoe ME, Hentzer M, Kristoffersen P, Kôte M, Nielsen J, Eberl L, Givskov M (2005) Screening for Quorum-Sensing Inhibitors (QSI) by Use of a Novel Genetic System, the QSI Selector. *J Bacteriol* 187:1799-1814.
18. Zhang R, Pappas T, Brace JL, Miller PC, Oulmasov T, Molyneaux JM, Anderson JC, Bashkin JK, Winans SC, Joachimiak A (2002) Structure of a bacterial quorum-sensing transcription factor complexed with pheromone and DNA. *Nature* 417:971-974.
19. Sjöblom S, Brader G, Koch G, Palva ET (2006) Cooperation of two distinct ExpR regulators controls quorum sensing specificity and virulence in the plant pathogen *Erwinia carotovora*. *Mol Microbiol* 60:1474-1489.
20. Fuqua WC, Winans SC, Greenberg EP (1994) Quorum sensing in bacteria: the LuxR-LuxI family of cell density-responsive transcriptional regulators. *J Bacteriol* 176:269.
21. Swem LR, Swem DL, Wingreen NS, Bassler BL (2008) Deducing Receptor Signaling Parameters from In Vivo Analysis: LuxN/AI-1 Quorum Sensing in *Vibrio harveyi*. *Cell* 134:461-473.
22. Galloway WRJD, Hodgkinson JT, Bowden SD, Welch M, Spring DR (2010) Quorum Sensing in Gram-Negative Bacteria: Small-Molecule Modulation of AHL and AI-2 Quorum Sensing Pathways. *Chem Rev* 111:28-67.
23. Geske GD, O'Neill JC, Blackwell HE (2008) Expanding dialogues: from natural autoinducers to non-natural analogues that modulate quorum sensing in Gram-negative bacteria. *Chem Soc Rev* 37:1432-1447.

- 1 24. Galloway WRJD, Hodgkinson JT, Bowden S, Welch M, Spring DR (2012) Applications of small
2 molecule activators and inhibitors of quorum sensing in Gram-negative bacteria. *Trends Microbiol*
3 20:449-458.
- 4 25. Skovstrup S, Quement L, Thordal S, Hansen T, Jakobsen TH, Harmsen M, Tolker-Nielsen T,
5 Nielsen TE, Givskov M, Taboureau O (2013) Identification of LasR Ligands through a Virtual
6 Screening Approach. *Chem Med Chem* 8:157-163.
- 7 26. Geske GD, Wezeman RJ, Siegel AP, Helen E (2005) Small molecule inhibitors of bacterial quorum
8 sensing and biofilm formation. *J Am Chem Soc* 127:12762-12763.
- 9 27. Geske GD, O'Neill JC, Miller DM, Mattmann ME, Helen E (2007) Modulation of bacterial quorum
10 sensing with synthetic ligands: systematic evaluation of N-acylated homoserine lactones in multiple
11 species and new insights into their mechanisms of action. *J Am Chem Soc* 129:13613-13625.
- 12 28. Estephane J, Dauvergne J, Soullère L, Reverchon S, Queneau Y, Doutheau A (2008) N -Acyl-3-
13 amino-5 H -furanone derivatives as new inhibitors of LuxR-dependent quorum sensing: Synthesis,
14 biological evaluation and binding mode study. *Bioorg Med Chem Lett* 18:4321-4324.
- 15 29. McInnis CE, Blackwell HE (2011) Thiolactone modulators of quorum sensing revealed through
16 library design and screening. *Bioorg Med Chem* 19:4820-4828.
- 17 30. Nasser W, Reverchon S (2007) New insights into the regulatory mechanisms of the LuxR family of
18 quorum sensing regulators. *Anal Bioanal Chem* 387:381-390.
- 19 31. Soullère L, Sabbah M, Fontaine F, Queneau Y, Doutheau A (2010) LuxR-dependent quorum
20 sensing: Computer aided discovery of new inhibitors structurally unrelated to N-acylhomoserine
21 lactones. *Bioorg Med Chem Lett* 20:4355-4358.
- 22 32. Sabbah M, Fontaine F, Grand L, Boukraa M, Efrat ML, Doutheau A, Soullère L, Queneau Y (2012)
23 Synthesis and biological evaluation of new N-acyl-homoserine-lactone analogues, based on triazole
24 and tetrazole scaffolds, acting as LuxR-dependent quorum sensing modulators. *Bioorg Med Chem*
25 20:4727-4736.
- 26 33. Soullère L, Frezza M, Queneau Y, Doutheau A (2007) Exploring the active site of acyl homoserine
27 lactones-dependent transcriptional regulators with bacterial quorum sensing modulators using
28 molecular mechanics and docking studies. *J Mol Graphics Model* 26:581-590.
- 29 34. Soullère L, Guilianni N, Queneau Y, Jerez CA, Doutheau A (2008) Molecular insights into quorum
30 sensing in *Acidithiobacillus ferrooxidans* bacteria via molecular modelling of the transcriptional
31 regulator AfeR and of the binding mode of long-chain acyl homoserine lactones. *J Mol Model* 14:599-
32 606.
- 33 35. Schrödinger Suite 2011 Protein Preparation Wizard; Epik version 2.2, Schrödinger, LLC, New
34 York, NY, 2011; Impact version 5.7, Schrödinger, LLC, New York, NY, 2011; Prime version 3.0,
35 Schrödinger, LLC, New York, NY, 2011.
- 36 36. Sadek MM, Serrya RA, Kafafy A-HN, Ahmed M, Wang F, Abouzid KAM (2013) Discovery of
37 new HER2/EGFR dual kinase inhibitors based on the anilinoquinazoline scaffold as potential anti-
38 cancer agents. *J Enzyme Inhib Med Chem* 1:1-8.
- 39 37. Ahmed M, Sadek MM, Serrya RA, Kafafy A-HN, Abouzid KA, Wang F (2013) Assessment of
40 new anti-HER2 ligands using combined docking, QM/MM scoring and MD simulation. *J Mol Graphics*
41 *Model* 40:91-98.
- 42 38. Prime version 3.0, Schrödinger, LLC, New York, NY, 2011.
- 43 39. Glide, version 5.7, Schrödinger, LLC, New York, NY, 2011.
- 44 40. Rocha GB, Freire RO, Simas AM, Stewart JJP (2006) RM1: A reparameterization of AM1 for H,
45 C, N, O, P, S, F, Cl, Br, and I. *J Comput Chem* 27:1101-1111.
- 46 41. Jaguar, version 7.8, Schrödinger, LLC, New York, NY, 2011.
- 47 42. Friesner RA, Murphy RB, Repasky MP, Frye LL, Greenwood JR, Halgren TA, Sanschagrin PC,
48 Mainz DT (2006) Extra Precision Glide:Docking and Scoring Incorporating a Model of Hydrophobic
49 Enclosure for Protein-Ligand Complexes. *J Med Chem* 49:6177-6196.
- 50 43. D.A. Case, T.A. Darden, T.E. Cheatham, III, C.L. Simmerling, J. Wang, R.E. Duke, R. Luo, R.C.
51 Walker, W. Zhang, K.M. Merz, B. Roberts, S. Hayik, A. Roitberg, G. Seabra, J. Swails, A.W. Goetz, I.
52 Kolossváry, K.F. Wong, F. Paesani, J. Vanicek, R.M. Wolf, J. Liu, X. Wu, S.R. Brozell, T.
53 Steinbrecher, H. Gohlke, Q. Cai, X. Ye, J. Wang, M.-J. Hsieh, G. Cui, D.R. Roe, D.H. Mathews, M.G.
54 Seetin, R. Salomon-Ferrer, C. Sagui, V. Babin, T. Luchko, S. Gusarov, A. Kovalenko, and P.A.
55 Kollman (2012), AMBER 12, University of California, San Francisco.
- 56 44. Duan Y, Wu C, Chowdhury S, Lee MC, Xiong G, Zhang W, Yang R, Cieplak P, Luo R, Lee T,
57 Caldwell J, Wang J, Kollman P (2003) A point-charge force field for molecular mechanics simulations

- of proteins based on condensed-phase quantum mechanical calculations. *J Comput Chem* 24:1999-2012.
45. M.J.Frisch et al. (2009) Gaussian09, Rev A.02, Gaussian Inc, Wallingford, CT.
46. Bayly CI, Cieplak P, Cornell W, Kollman PA (1993) A well-behaved electrostatic potential based method using charge restraints for deriving atomic charges: the RESP model. *J Phys Chem* 97:10269-10280.
47. Wang J, Wolf RM, Caldwell JW, Kollman PA, Case DA (2004) Development and testing of a general amber force field. *J Comput Chem* 25:1157-1174.
48. Jorgensen WL, Chandrasekhar J, Madura JD, Impey RW, Klein ML (1983) Comparison of simple potential functions for simulating liquid water. *J Chem Phys* 79:926-935.
49. Ryckaert J-P, Ciccotti G, Berendsen HJC (1977) Numerical integration of the cartesian equations of motion of a system with constraints: molecular dynamics of n-alkanes. *J Comput Phys* 23:327-341.
50. Berendsen HJC, Postma JPM, van Gunsteren WF, DiNola A, Haak JR (1984) Molecular dynamics with coupling to an external bath. *J Chem Phys* 81:3684-3690.
51. Darden T, York D, Pedersen L (1993) Particle mesh Ewald: An N.log(N) method for Ewald sums in large systems. *J Chem Phys* 98:10089-10092.
52. Miller BR, McGee TD, Swails JM, Homeyer N, Gohlke H, Roitberg AE (2012) MMPBSA.py: An Efficient Program for End-State Free Energy Calculations. *Journal of Chemical Theory and Computation* 8:3314-3321.
53. Schwobel J, Ebert R, Kuhne R, Schuurmann G (2009) Prediction of the Intrinsic Hydrogen Bond Acceptor Strength of Chemical Substances from Molecular Structure. *J Phys Chem A* 113:10104-10112.
54. Ho BK, Agard DA (2009) Probing the flexibility of large conformational changes in protein structures through local perturbations. *PLoS Comp Biol* 5:1000343.
55. Stauff DL, Bassler BL (2011) Quorum Sensing in *Chromobacterium violaceum*: DNA Recognition and Gene Regulation by the CviR Receptor. *J Bacteriol* 193:3871-3878.
56. Voter AF (1997) A method for accelerating the molecular dynamics simulation of infrequent events. *The Journal of Chemical Physics* 106:4665-4677.
57. Lefèvre F, Rémy M-H, Masson J-M (1997) Alanine-stretch scanning mutagenesis: a simple and efficient method to probe protein structure and function. *Nucleic Acids Res* 25:447-448.
58. Morrison KL, Weiss GA (2001) Combinatorial alanine-scanning. *Curr Opin Chem Biol* 5:302-307.

Table 1: Selected binding energy scores together with the *in vitro* measured IC₅₀ values for the inhibitors under study ranked according to the XP Gscore.

Inhibitors	IC ₅₀ (μ M) ^a	XP GScore	XP LipophilicEvdW	XP Electrostatic	Glide Emodel	Prime MMGBSA DG bind	Prime MMGBSA DG bind vdW
L14		-10.28	-4.90	-1.16	-91.15	-99.19	-49.53
L15		-10.25	-5.12	-1.19	-96.06	-102.41	-47.95
L12		-10.02	-4.19	-1.19	-89.99	-100.53	-46.46
L11		-9.71	-4.66	-1.19	-93.41	-116.59	-51.84
L4		-9.50	-4.60	-1.20	-94.81	-98.70	-45.54
L3	0.38	-9.49	-4.63	-1.20	-90.40	-105.54	-46.19
TL12	0.63	-9.43	-4.14	-1.07	-80.56	-104.45	-44.09
L9		-9.40	-4.50	-1.18	-96.34	-107.02	-48.73
L13		-9.40	-4.40	-1.21	-70.66	-101.06	-47.33
L5		-9.38	-4.64	-1.17	-95.11	-106.60	-48.48
L8		-9.36	-4.48	-1.17	-92.92	-102.88	-44.60
TL15	5.00	-9.34	-4.76	-1.09	-89.31	-102.13	-46.57
L2		-9.34	-4.29	-1.18	-91.56	-94.47	-43.61
TL14	4.00	-9.32	-4.50	-1.05	-83.97	-101.76	-46.95
TL1		-9.11	-4.27	-1.18	-89.77	-92.72	-43.31
TL11	1.40	-9.08	-4.49	-1.09	-86.47	-118.22	-51.14
L10		-8.76	-4.31	-1.10	-72.97	-99.16	-45.17
TL3	1.10	-8.61	-4.19	-1.05	-79.07	-104.49	-45.00
TL4	1.80	-8.60	-4.25	-1.07	-82.58	-101.97	-45.27
TL2	2.10	-8.58	-3.86	-1.06	-81.62	-100.98	-39.87
TL5	1.40	-8.53	-4.27	-1.07	-83.29	-102.32	-45.68
TL8	2.10	-8.51	-3.97	-0.98	-81.19	-115.31	-48.53
TL9	2.70	-8.36	-4.11	-1.04	-80.41	-109.05	-41.12
TL13	3.40	-8.20	-3.75	-1.02	-69.40	-95.52	-40.07
TL1	2.60	-8.18	-3.91	-1.07	-79.01	-96.20	-42.11
L6		-8.05	-3.92	-1.13	-77.15	-90.41	-42.70
L7		-7.81	-4.26	-1.09	-74.02	-99.39	-44.11
L16		-7.78	-4.66	-1.18	-76.10	-101.75	-48.56
TL10	37.00	-7.67	-3.92	-0.94	-70.76	-97.99	-37.71
TL6	2.50	-7.29	-4.12	-1.14	-75.55	-112.28	-47.43
TL7	11.00	-6.95	-4.05	-0.88	-65.21	-98.33	-38.84
TL16	3.90	-5.69	-3.95	-0.84	-77.05	-109.95	-49.65
$r_{\text{(Pearson)}}^b$		0.30	0.25	0.44	0.49	0.34	0.52

^aSee Ref. [8].

^b Pearson correlation coefficient between the *in silico* calculated docking scores and the *in vitro* measured IC₅₀ values.

Table 2: Total and decomposed binding energies of the MD studied complexes (kcal·mol⁻¹) together with the experimental IC₅₀ values.

Contribution	Inhibitor	
	L3	TL3
ΔE_{ele}	-33.54	-28.37
ΔE_{vdw}	-45.31	-46.56
$\Delta E_{\text{binding-gas}}^{\text{a}}$	-78.85	-74.93
$\Delta G_{\text{binding}}(\text{AMBER-PBSA})^{\text{b}}$	-63.54	-59.11
$\Delta G_{\text{binding}}(\text{AMBER-GBSA})^{\text{b}}$	-48.65	-47.60

$$^{\text{a}}\Delta E_{\text{binding-gas}} = \Delta E_{\text{ele}} + \Delta E_{\text{vdw}}$$

$$^{\text{b}}\Delta G_{\text{binding}} = \Delta E_{\text{ele}} + \Delta E_{\text{vdw}} + \Delta G_{\text{solvation}}$$

Figure captions

Figure 1: Two dimensional (2D) structures of the lactone (X=O) and thiolactone (X=S) inhibitors under study.

Figure 2: Three dimensional (3D) ribbon representation for the CviR monomer. Solid surface in the LBD represent the exact binding location of the inhibitors.

Figure 3: 2D ligand interaction diagrams for (a) a potential CviR antagonist (PDB code: 3QP5) and (b) a potential CviR agonist (PDB code: 3QP1).

Figure 4: 2D and 3D ligand interactions for some selected inhibitors under study in the CviR binding site (a) L12, (b) TL12 and (c) L14.

Figure 5: RMSD plots for the protein backbone C α atoms during the 30 ns production simulation for (a) dimer complexes and (b) monomer complexes.

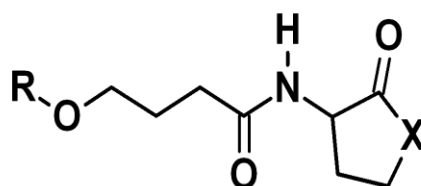
Figure 6: Per-residue heavy atoms RMSF plots during the 30 ns production simulation for (a) dimer complexes and (b) monomer complexes.

Figure 7: Selected H-bonds distances monitored during the 30 ns production simulations for (a, c) dimer complexes and (b, d) monomer complexes.

Figure 8: 3D representation for (a) **L3** and (b) **TL3** with the surrounding amino acid residues. These two snapshots were obtained at the end of the 30 ns production simulations.

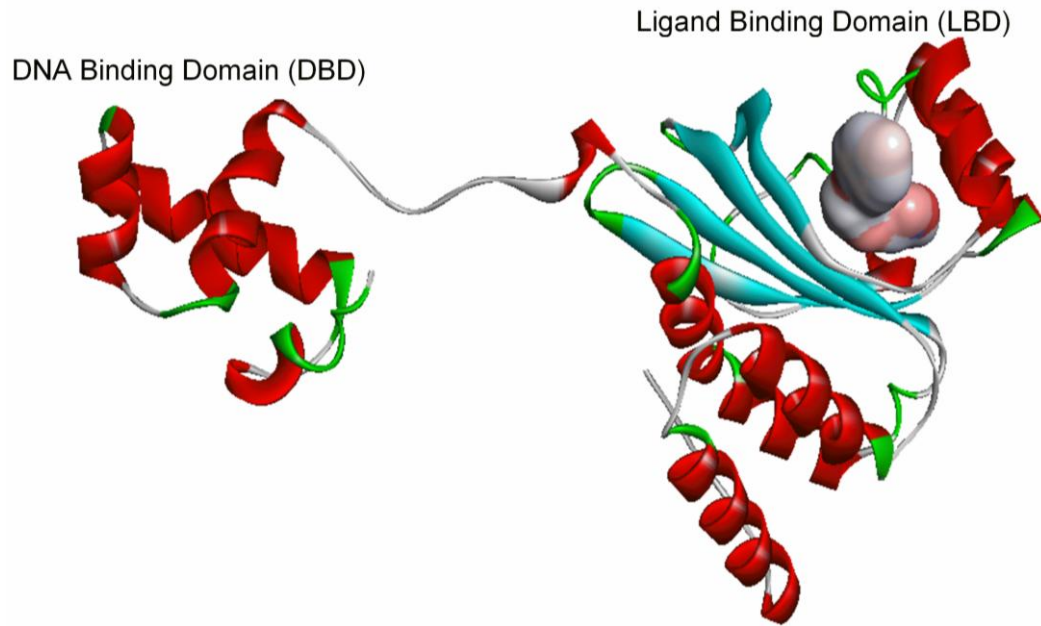
Figure 9: Per-residue binding energy decompositions calculated using the MMPBSA module of AMBER, (a) per-residue contribution to the vdW interaction term and (b) per-residue contribution to the electrostatic interaction term.

Figure 1: Two dimensional (2D) structures of the lactone (X=O) and thiolactone (X=S) inhibitors under study.



TL1(L1)	X = S (O)	R=		TL10(L10)	X = S (O)	R=	
TL2(L2)	X = S (O)	R=		TL11(L11)	X = S (O)	R=	
TL3(L3)	X = S (O)	R=		TL12(L12)	X = S (O)	R=	
TL4(L4)	X = S (O)	R=		TL13(L13)	X = S (O)	R=	
TL5(L5)	X = S (O)	R=		TL14(L14)	X = S (O)	R=	
TL6(L6)	X = S (O)	R=		TL15(L15)	X = S (O)	R=	
TL7(L7)	X = S (O)	R=		TL16(L16)	X = S (O)	R=	
TL8(L8)	X = S (O)	R=					
TL9(L9)	X = S (O)	R=					

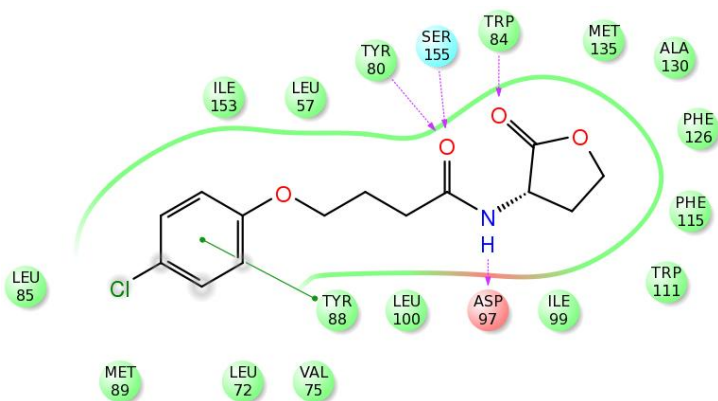
Figure 2: Three dimensional (3D) ribbon representation for the CviR monomer. Solid surface in the LBD represent the exact binding location of the inhibitors.



1
2
3
4
5
6
7
8
9
10
11
12
13
14
15
16
17
18
19
20
21
22
23
24
25
26
27
28
29
30
31
32
33
34
35
36
37
38
39
40
41
42
43
44
45
46
47
48
49
50
51
52
53
54
55
56
57
58
59
60
61
62
63
64
65

Figure 3: 2D ligand interaction diagrams for (a) a potential CviR antagonist (PDB code: 3QP5) and (b) a potential CviR agonist (PDB code: 3QP1).

(a)



(b)

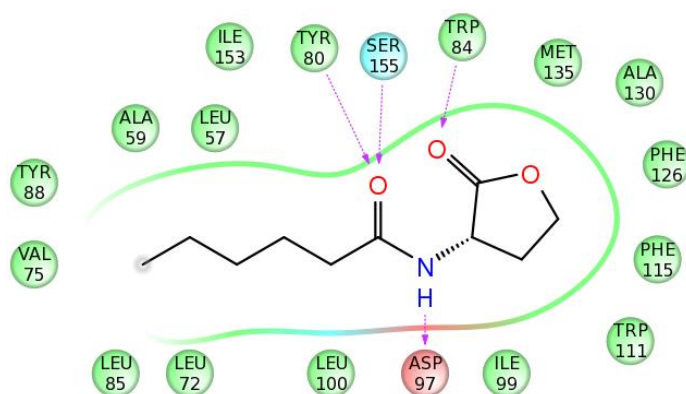
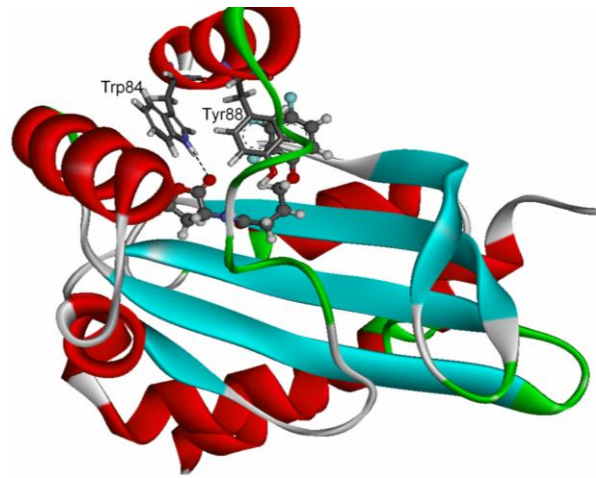
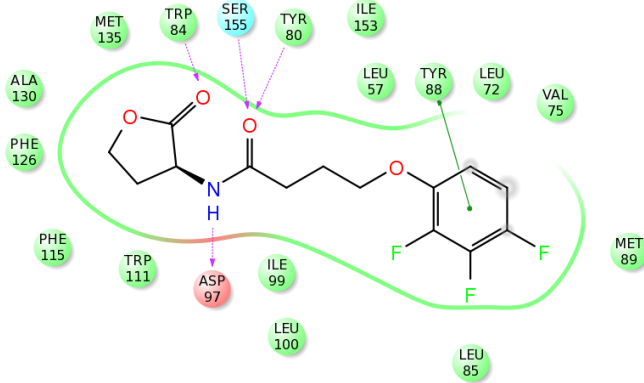
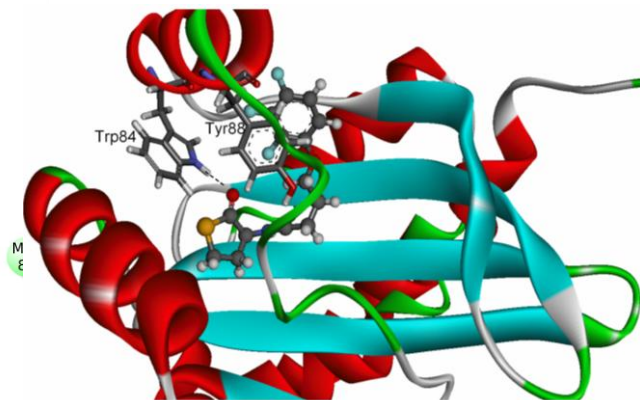
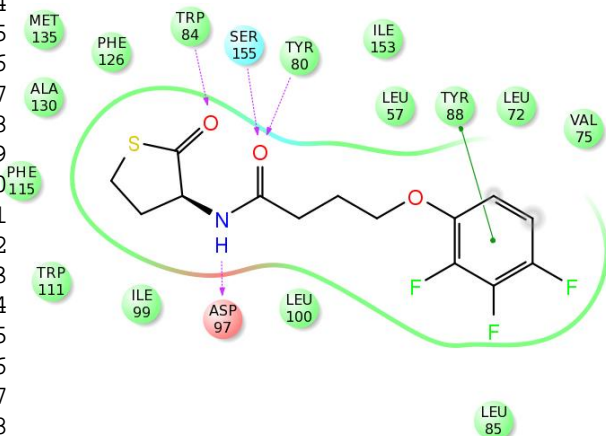


Figure 4: 2D and 3D ligand interactions for some selected inhibitors under study in the CviR binding site (a) L12, (b) TL12 and (c) L14.

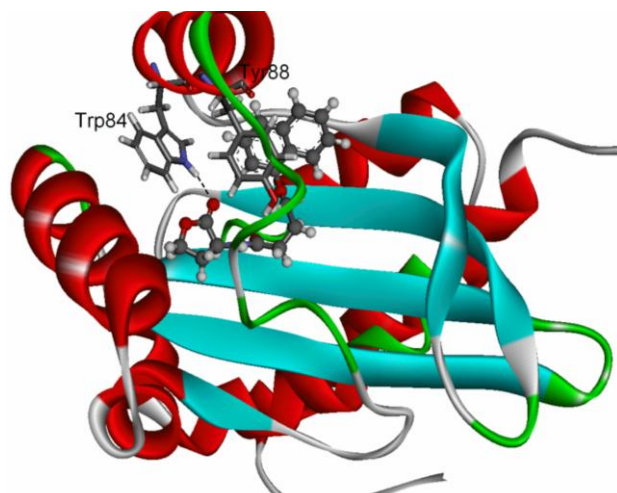
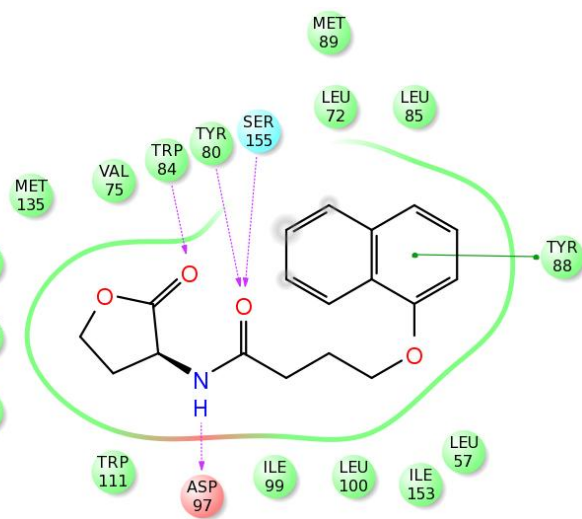
(a)



(b)



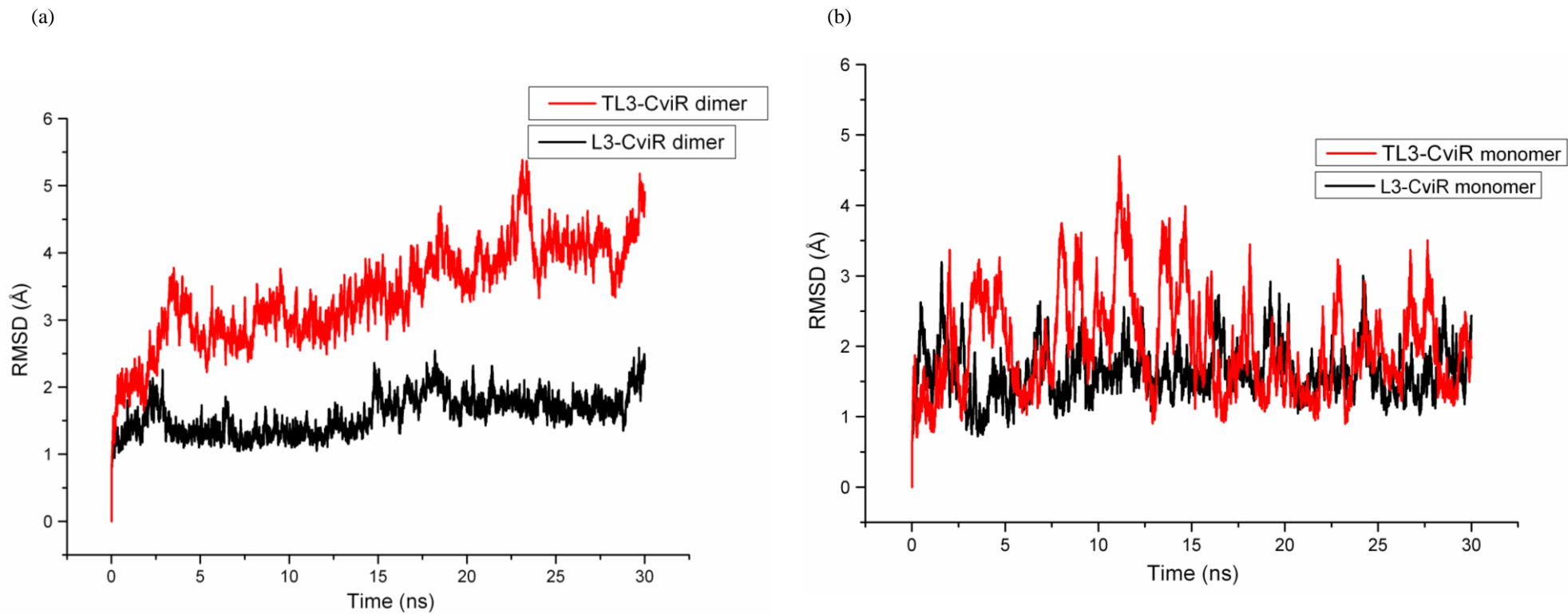
(c)



1
2
3
4
5
6
7
8
9
10
11
12
13
14
15
16
17
18
19
20
21
22
23
24
25
26
27
28
29
30
31
32
33
34
35
36
37
38
39
40
41
42
43
44
45
46
47
48
49
50
51
52
53
54
55
56
57
58
59
60
61
62
63
64
65

1
2
3
4
5
6
7
8
9
10
11
12
13
14
15
16
17
18
19
20
21
22
23
24
25
26
27
28
29
30
31
32
33
34
35
36
37
38
39
40
41
42
43
44
45
46
47
48
49

Figure 5: RMSD plots for the protein backbone C α atoms during the 30 ns production simulation for (a) dimer complexes and (b) monomer complexes.



1
2
3
4
5
6
7
8
9
10
11
12
13
14
15
16
17
18
19
20
21
22
23
24
25
26
27
28
29
30
31
32
33
34
35
36
37
38
39
40
41
42
43
44
45
46
47
48
49

Figure 6: Per-residue heavy atoms RMSF plots during the 30 ns production simulation for (a) dimer complexes and (b) monomer complexes.

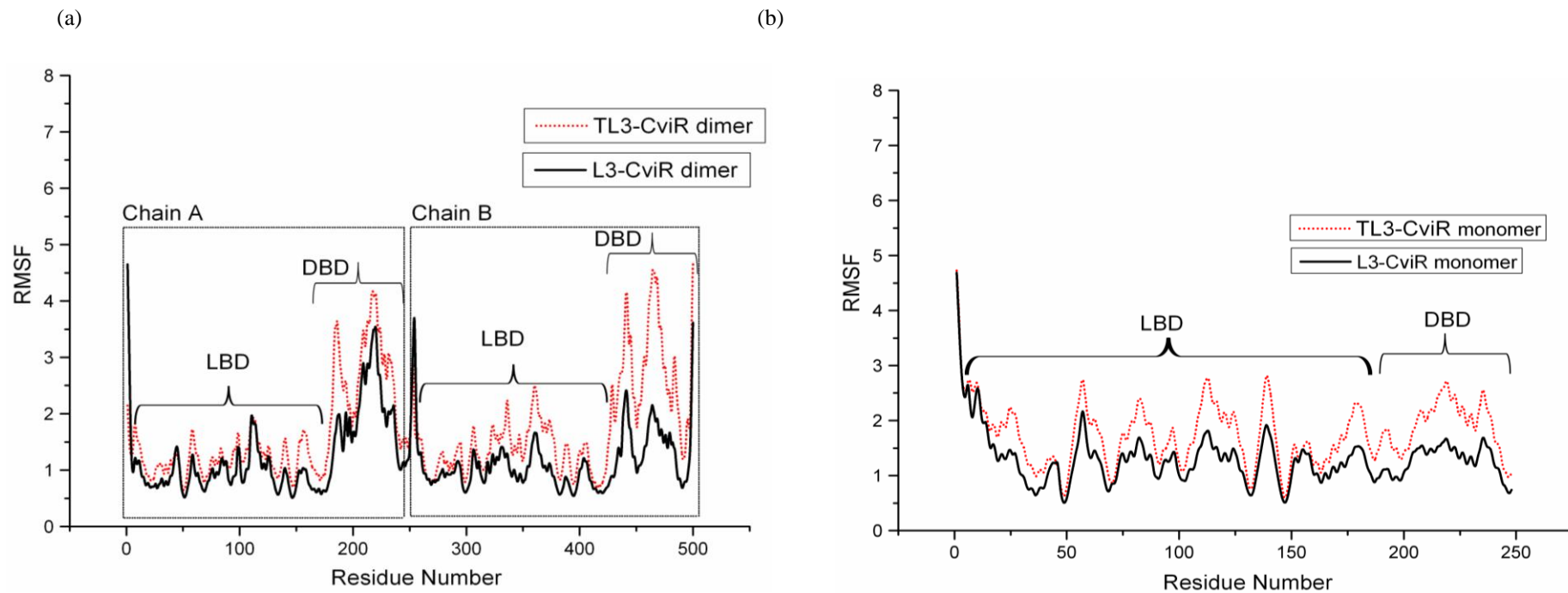
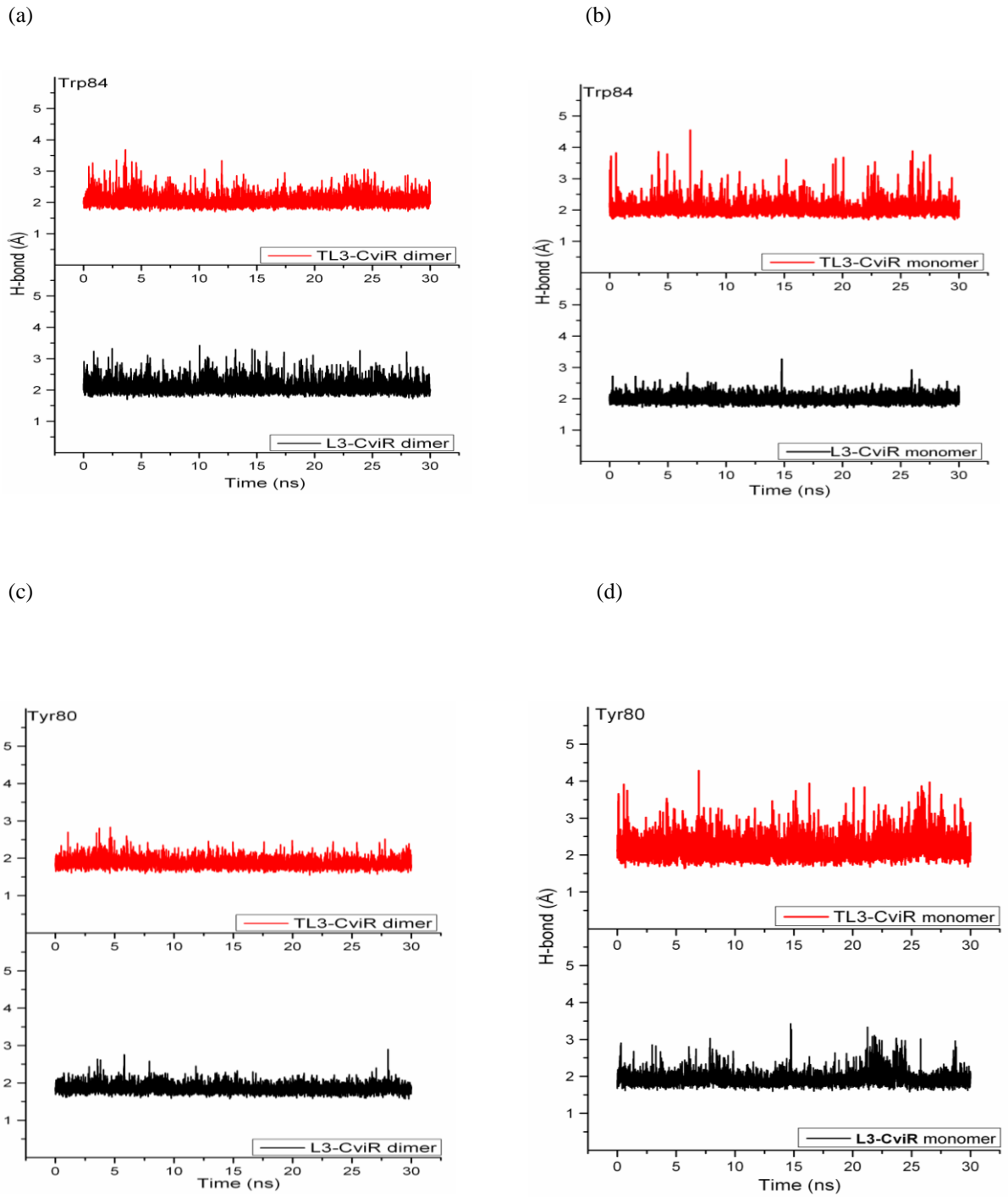


Figure 7: Selected H-bonds distances monitored during the 30 ns production simulations for (a, c) dimer complexes and (b, d) monomer complexes.



1
2
3
4
5
6
7
8
9
10
11
12
13
14
15
16
17
18
19
20
21
22
23
24
25
26
27
28
29
30
31
32
33
34
35
36
37
38
39
40
41
42
43
44
45
46
47
48
49

Figure 8: 3D representation for (a) L3 and (b) TL3 with the surrounding amino acid residues. These two snapshots were obtained at the end of the 30 ns production simulations.

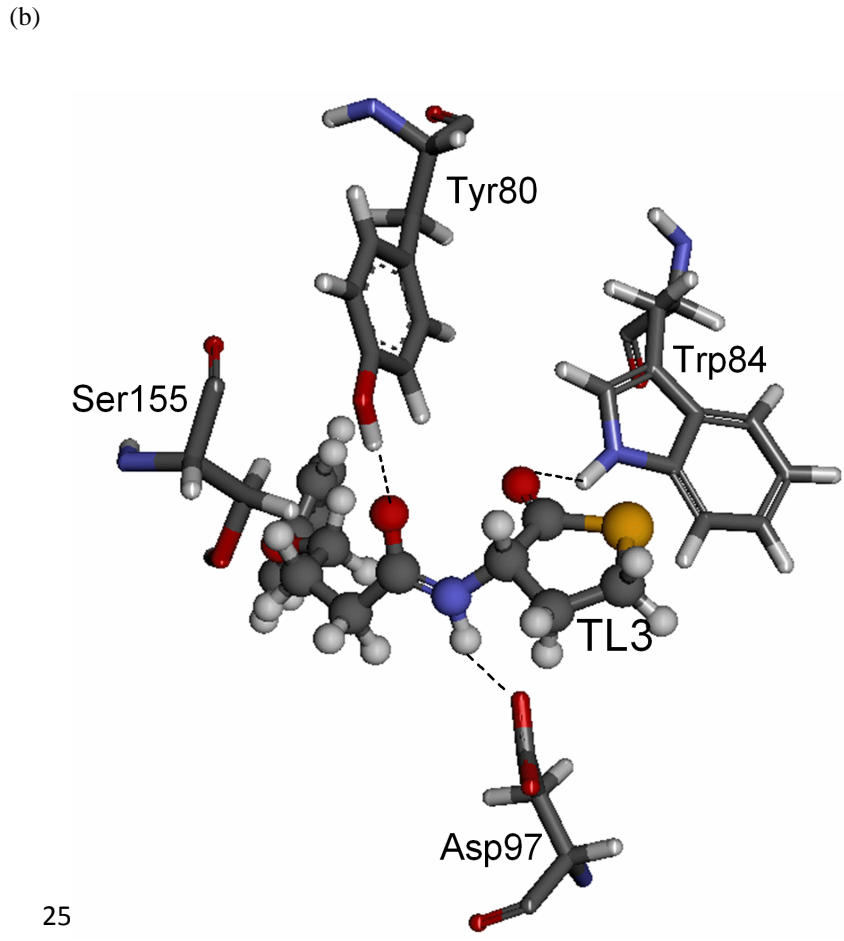
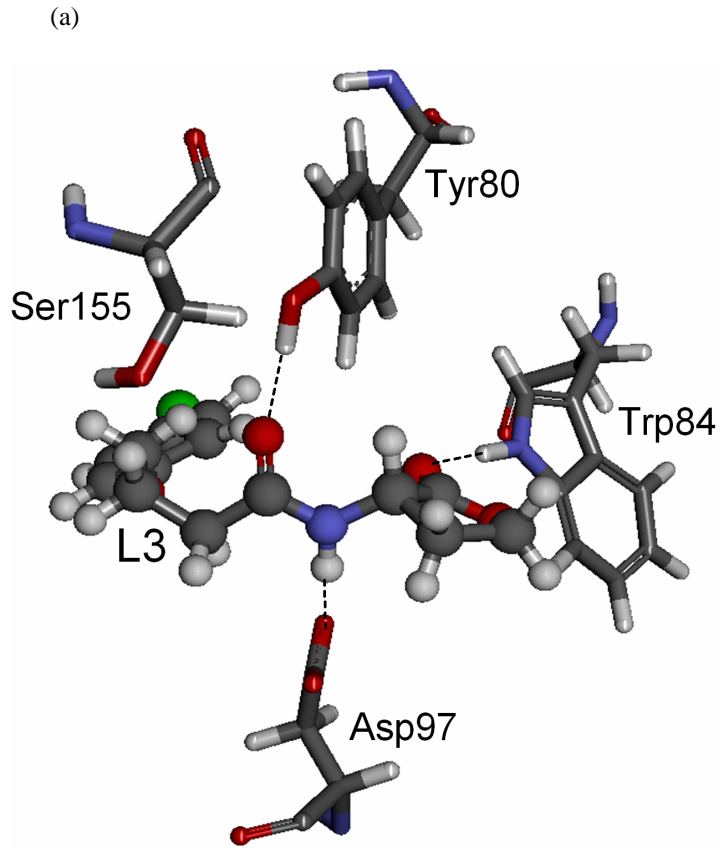
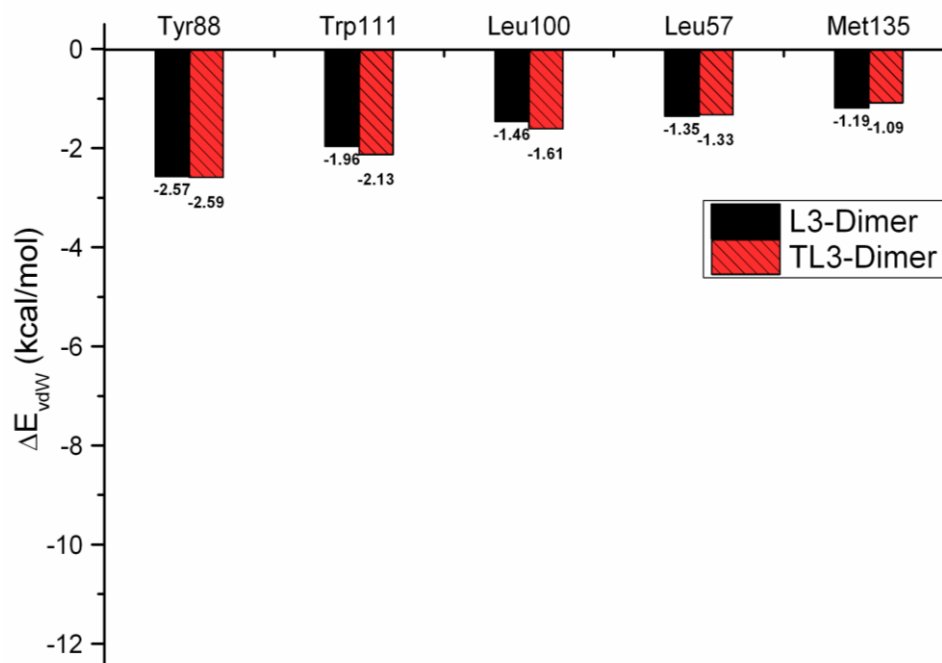


Figure 9: Per-residue binding energy decompositions calculated using the MMPBSA module of AMBER, (a) per-residue contribution to the vdW interaction term and (b) per-residue contribution to the electrostatic interaction term.

(a)



(b)

